Hindawi Publishing Corporation
Advances in Materials Science and Engineering
Volume 2015, Article ID 626429, 7 pages
http://dx.doi.org/10.1155/2015/626429

*Research Article*

# $TiC_{0.5}N_{0.5}$-Based Cermets with Varied Amounts of $Si_3N_4$ Nanopowders Prepared by Spark Plasma Sintering

**Changchun Lv, Zhijian Peng, Zhiqiang Fu, and Chengbiao Wang**

*Key Laboratory on Deep GeoDrilling Technology of the Ministry of Land and Resources, School of Engineering and Technology, China University of Geosciences, Beijing 100083, China*

Correspondence should be addressed to Zhijian Peng; pengzhijian@cugb.edu.cn

Received 1 October 2014; Revised 11 January 2015; Accepted 20 January 2015

Academic Editor: Achim Trampert



TiCN-based cermets with varied fractions of $Si_3N_4$ nanopowder (0–5 wt.%) were prepared by spark plasma sintering. The microstructural and mechanical properties of these cermets were investigated. In general, with increasing addition amount of $Si_3N_4$ nanopowder the relative density as well as mechanical properties of the as-prepared TiCN cermets increased first and then decreased. The samples containing 2 wt.% $Si_3N_4$ nanopowder presented the best performance with the relative density of about 98%, bending strength of 1000 MPa, and Vickers microhardness of about 1810 $HV_{10}$.

## 1. Introduction

TiCN-based cermets have attracted extensive attention as cutting tools, moulds, and various wear-resistant components. They are known to possess higher hardness and better chemical stability in some respects than traditional WC-based hard metals [1–7]. However, their lower toughness still limits their potentially wider application. Given that, most studies have focused on the strengthening and toughening of such kind of materials, in which some tried to produce nanosized or ultra-fine cermets based on the well-known Hall-Patch equation: the smaller TiCN grains the higher cermet hardness and strength [8–10], and others added some second phases like metal carbides [11–13] or nanoadditives into the cermet matrix [14–16].

Spark plasma sintering (SPS) is a kind of fast sintering process, which is known for its relatively low sintering temperature and high heating rate. During sintering, the grain growth could be suppressed, which is in favor of improving the mechanical properties of engineering materials. Consequently, it has been increasingly used in preparing various composites [17–22]. However, there was no report about TiCN-based cermets with $Si_3N_4$ nanopowders prepared by SPS.

Thus, in this study, SPS was used to fabricate TiCN-based cermets with varied fractions of $Si_3N_4$ nanopowders. The addition effect of $Si_3N_4$ nanopowder on the microstructure and mechanical properties of the as-prepared cermets were investigated, and the strengthening mechanism was also probed.

## 2. Experimental Procedure

*2.1. Sample Preparation.* Commercially available $TiC_{0.5}N_{0.5}$, WC, Mo, Ni, and VC powders were used as starting powders, and their specifications were listed in Table 1. In order to explore the effect of $Si_3N_4$ addition on the microstructure and mechanical properties of TiCN-based cermets, the added $Si_3N_4$ content was varied from 0 to 5 wt.% in increment of 1 wt.%. The cermet compositions designed in this work were 74 wt.% $TiC_{0.5}N_{0.5}$ + 10 wt.% WC + 10 wt.% Ni + 5 wt.% Mo + 1 wt.% VC with extra addition of different amounts of nanosized $Si_3N_4$ powder.

During sample preparation, all the raw powders except $Si_3N_4$ nanopowder were firstly mixed together and ball-milled thoroughly in an attrition mill (Model: SY-1, China) for $1.278 \times 10^5$ s using YG-6 WC balls (ISO: k20) as grinding media and absolute alcohol as dispersion media. Following that, the designed amount of $Si_3N_4$ nanopowder was added into the slurry for another 1.8 ks milling. Shortly, the mixed slurry was dried off in a vacuum oven at 338–368 K under a

Table 1: Specifications of the initial powders used for the preparation of TiCN-based cermets.

| | Purity (wt.%) | Oxygen content (wt.%) | Particle size ($\mu$m) |
|---|---|---|---|
| $TiC_{0.5}N_{0.5}$ | >99.5 | <0.46 | 0.5 |
| WC | >99.5 | <0.31 | 1.8–2.2 |
| Nano-$Si_3N_4$ | >99.0 | <0.12 | 0.1–0.3 |
| Ni | >99.9 | — | 0.1–2 |
| Mo | >99.9 | <0.05 | <2.0 |
| VC | >99.5 | <0.2 | 2.0–4 |

Table 2: Lattice constant of Ni in the as-prepared TiCN-based cermets.

| Samples | Lattice constant of Ni |
|---|---|
| TiCN-0 wt.% $Si_3N_4$ | 3.5309 |
| TiCN-1 wt.% $Si_3N_4$ | 3.5213 |
| TiCN-2 wt.% $Si_3N_4$ | 3.5156 |
| TiCN-3 wt.% $Si_3N_4$ | 3.5138 |
| TiCN-4 wt.% $Si_3N_4$ | 3.5095 |
| TiCN-5 wt.% $Si_3N_4$ | 3.5072 |

pressure of 0.1 Pa. After that, the powder chunks were pestled and sieved into fine powder, and the powders were sintered in graphite dies by a SPS apparatus (Model: SPS-1050T, Japan). For the sintering, the samples were heated up to 1623 K with a heating rate of 473 K/min under a pressure of about 30 MPa, and the soaking time was 8 min. Finally, the samples were cooled down by furnace cooling, acquiring disks with a final dimension of Φ20 mm × 5 mm.

*2.2. Materials Characterization.* The cermet disks were first sectioned into small bars with dimension of 2 mm × 3 mm × 10 mm and polished to a mirror surface. Then, using the polished bars, the flexural strength was evaluated on a Zwick/Z005 tester by a three-point bending experiment. During the testing, a loading rate of 0.5 mm/min was applied. With the broken bars after the measurement of flexural strength, the bulk densities of the cermet specimens were evaluated by Archimedes method according to international standard (ISO18754). Then the final relative densities were estimated in accordance with the rule of mixtures.

The measurement of specimen hardness was taken from the central part of the polished bars. The Vickers hardness test was performed at room temperature on a microhardness tester (Model: VH-5, China) with an indenting load of 10 kgf and a dwelling time of 20 s. Five microindentations were conducted at different locations on the polished cermets, and the reported value here is the average of the measured hardnesses.

The microstructure was examined on both the polished and fracture surfaces of the samples by scanning electron microscopy (SEM, Model: JSM-7410LV, Japan). The content of each element was recorded by an energy dispersive X-ray (EDX) spectroscopy attached to the SEM. The phase compositions of the samples were identified by X-ray diffraction (XRD) on a D8-advance X-ray diffractometer (Cu Ka, $\lambda$ = 1.5418 Å) under continuous scanning mode with a speed of 5°/min.

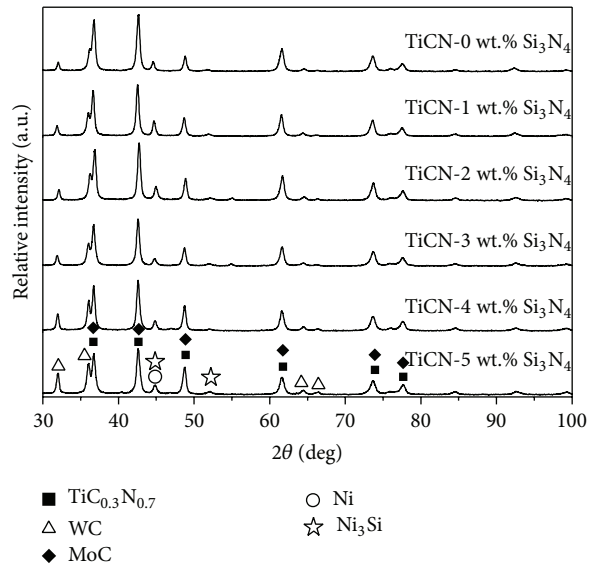


Figure 1: Typical XRD patterns of the as-prepared TiCN-based cermets with different amounts of $Si_3N_4$ nanopowder.

## 3. Results and Discussion

*3.1. Phase Composition and Microstructure.* Figure 1 illustrates typical XRD patterns of the as-prepared TiCN-based cermets with different amounts of $Si_3N_4$ nanopowder. By XRD, WC (JCPDS card: 65-8828), $TiC_{0.3}N_{0.7}$ (JCPD: 42-1488), Ni (JCPDS: 65-0380), and MoC (JCPDS: 65-0280) phases were identified in each sample. However, no diffraction peaks of $Si_3N_4$ were identified, possibly due to the small addition amount of $Si_3N_4$ nanopowder that cannot be detected by XRD in the detection limit, or some reactions happened during sintering that consumed out the added $Si_3N_4$ nanopowder. In addition, it can be found that one of the diffraction peaks, that of Ni(111) grain plane, shifts to high diffraction angle with increasing addition of $Si_3N_4$ nanopowder. As a result, a new phase, namely, $Ni_3Si$ (JCPDS: 65-3243) phase can be identified. Also, via further calculation of the lattice constant of Ni (listed in Table 2), it can be found that the value of the so-called Ni lattice constant decreases following the increased addition amount of $Si_3N_4$ nanopowder, implying that some of Si atoms are merging into Ni, since it is known that the atomic size of Ni is much larger than that of Si. Taking all these information into account, it is rational to deduce that $Si_3N_4$ had reacted with N, generating $Ni_3Si$.

Typical SEM images in backscattering electron (BSE) mode on polished surface of the as-prepared samples with different amounts of $Si_3N_4$ nanopowder are shown in Figure 2. From this figure, it could be observed that there were almost no pores in each sample, revealing the fully dense structures of the samples after sintering. As the addition

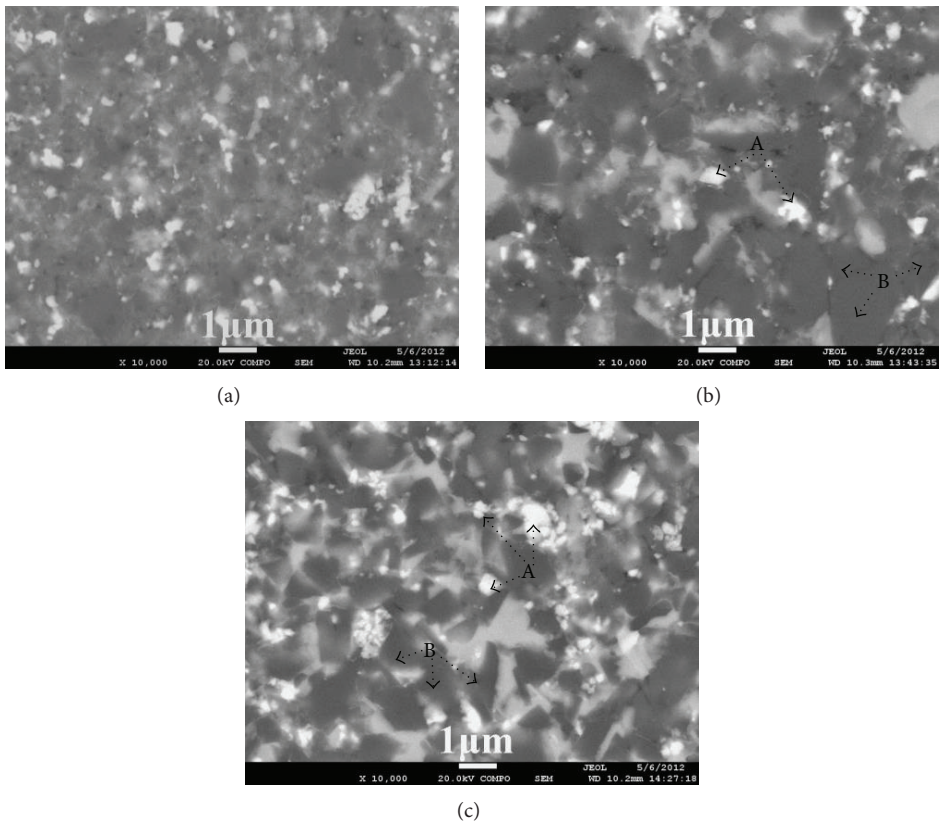


(a) (b)

(c)

Figure 2: Typical BSE SEM images on polished surface of the as-prepared samples with different amounts of $Si_3N_4$ nanopowder: (a) 0 wt.%, (b) 2 wt.%, and (c) 5 wt.%.

Table 3: Typical atomic content of each element in Particle A.

| Samples | C | N | Ti | V | Ni | Mo | W |
|---|---|---|---|---|---|---|---|
| TiCN-0 wt.% $Si_3N_4$ | 52.60 | 4.03 | 16.55 | 0.22 | 8.21 | 8.73 | 9.66 |
| TiCN-2 wt.% $Si_3N_4$ | 53.61 | 8.52 | 17.91 | 0.47 | 1.83 | 5.19 | 12.45 |
| TiCN-5 wt.% $Si_3N_4$ | 54.51 | 11.43 | 10.72 | 0.21 | 8.40 | 4.01 | 10.72 |

amount of $Si_3N_4$ nanopowder increased, the size of TiCN grains increased first and then decreased, and the number of small white particles (which was labeled as A) increased. Besides, the white particles tended to be located at the boundaries between black grains (which was labeled as B) or their triangle boundaries. As is known [1, 23], there are typical core-rim microstructure in TiCN-based cermets, and in the SEM images taken under BSE mode, they are most possibly black cores and white rims and/or sometimes white cores and grey rims. And, commonly, the black cores are considered as TiCN, while the white cores are (Ti,W,M)(C,N) (M=Mo, Ni, Ta, and so forth). In this work, however, the typical core-rim structure of TiCN cermets could not be found, which might be attributed to the fast sintering speed of SPS, during which the core-rim structure could not be formed completely and timely. As a result, there are some white particles (labeled as As) and black ones (labeled as Bs) as shown in Figure 2. As is well-known [1], the heavy metal elements such as W and Mo present a higher brightness. Typical atomic content of each element in Particles As and Bs is summarized in Tables 3 and 4, respectively, from which it could be seen that after increasing addition of $Si_3N_4$ nanopowder C and N contents in white particles increased; Ni and Si contents in black ones increased as well; however, Ti and C contents in black ones decreased. Above all, a tentative inference on this result was conducted that more and more Ni and Si would resolve into the hard TiCN phase, following the increasing addition of $Si_3N_4$ nanopowder, which is basically consistent with the XRD observation.

Figure 3 illustrates the densities of the as-prepared TiCN-based cermets as a function of mass fraction of $Si_3N_4$ nanopowder. It reveals that the apparent density decreased with increasing addition amount of $Si_3N_4$ nanopowder, while the relative density of the samples increased first and then decreased following the increasing addition amount of $Si_3N_4$ nanopowder, reaching its maximum of about 98% when the addition amount was 2.0 wt.%. Due to the lower density of $Si_3N_4$ (which is much lower than those of other ingredients in the cermets), the apparent density was reduced with increasing addition amount of $Si_3N_4$ nanopowder. But the

Table 4: Typical atomic content of each element in Particle B.

| Samples | C | N | Si | Ti | V | Ni | Mo | W |
|---|---|---|---|---|---|---|---|---|
| TiCN-0 wt.% $Si_3N_4$ | 41.05 | 13.17 | 0 | 42.53 | 0.16 | 0.45 | 1.89 | 0.75 |
| TiCN-2 wt.% $Si_3N_4$ | 39.03 | 19.52 | 0.15 | 35.51 | 0.01 | 1.88 | 2.99 | 0.91 |
| TiCN-5 wt.% $Si_3N_4$ | 34.91 | 25.91 | 0.29 | 34.11 | 0.15 | 2.10 | 1.77 | 0.76 |

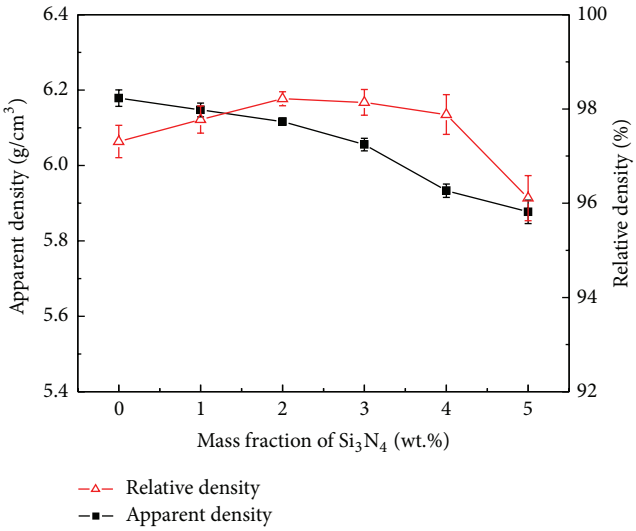


Figure 3: Apparent and relative densities of the as-prepared TiCN-based cermets as a function of mass fraction of $Si_3N_4$ nanopowder.

increase in relative density of the samples after the addition of small amount of $Si_3N_4$ nanopowder was attributed to the fact that the added $Si_3N_4$ nanopowder could be of benefit to the sintering, promoting the sample densification during sintering. However, when the addition amount of $Si_3N_4$ nanopowder becomes greater (more than 2 wt.%), the sample relative density dropped down on account of two reasons: the first one was that the formation of ceramic $Ni_3Si$ suppressed the plastic deformation of metal binder phase, and with more and more $Ni_3Si$, it became harder for the binder phase to perfectly wet the hard phase grains, resulting in reduced relative density; and another one was that the agglomeration owing to too much of the added nanosized powder was detrimental to the complete compaction of samples, and as a result, the relative density decreased.

Figure 4 displays typical second electron (SE) SEM images on the fracture surface of the prepared cermets with different amounts of $Si_3N_4$ nanopowder. It can be seen from this figure that the fracture mode of the prepared cermets did not change much even after $Si_3N_4$ nanopowder was added, which was still a mixture of intergranular and transgranular fractures. However, when comparing Figure 4(a) with Figure 4(b), it is interesting to see that there were more concave-convex tearing edges in the latter. In other words, when the fracture in such samples occurred, it dissipated more energy, indicating that the bond between the grains in the samples was strengthened. Moreover, when comparing Figure 4(b) with Figure 4(c), there was much more transgranular fracture and something like spalling occurred in the latter, implying that the bond between the particles in such samples became weak. From these phenomena it is reasonable to conclude that the addition of $Si_3N_4$ nanopowder with an appropriate amount is of benefit to bind the cermet grains; otherwise, that with too much of $Si_3N_4$ nanopowder is of disadvantage.

*3.2. Mechanical Properties.* Figure 5 presents the Vickers hardness of the as-prepared TiCN-based cermets as a function of mass fraction of $Si_3N_4$ nanopowder. It can be seen that the sample hardness increased first and then decreased with increasing addition of $Si_3N_4$ nanopowder, reaching its maximum of about 1810 $HV_{10}$ when its added amount was 2.0 wt.%. The whole change tendency in hardness was quite the same as that of the sample relative density, because it is well-known that the higher relative density, the higher hardness [24]. In the present work, besides the increased relative density, the boosted hardness could be also attributed to the desirable role of moderate amount of the resultant $Ni_3Si$ in improving the sample hardness. When the addition amount of $Si_3N_4$ nanopowder was small (approximately less than 2 wt.%), the white particles as shown in Figure 2 in the cermets became more after the addition of $Si_3N_4$ and the content of Ti, C, and N in white particles increased as well, indicating that the content of TiCN in white particles turned to be more. As a result, the whole hardness of the cermets was enhanced. As the addition amount of $Si_3N_4$ nanopowder increased (more than 2 wt.%), the hardness, however, turned to go down, not merely because of the decreased relative density as illustrated in Figure 4, but also owing to the increased contents of Ni and Si in the black particles as well as the increased amount of the black particles. Moreover, the hardness of $Ni_3Si$ is much lower than that of TiCN, which also contributed to the decrease in sample hardness. In addition, the weak binding strength (which can be seen from Figure 4(c)) between the particles also went against the improvement in hardness. For all these reasons, the sample hardness went down when too much of $Si_3N_4$ nanopowder was added.

Figure 6 shows the bending strength of the as-prepared cermets as a function of mass fraction of $Si_3N_4$ nanopowder. It can be seen that the bending strength of the samples went up first and then fell down, reaching its maximum of about 1000 MPa also when the added amount of $Si_3N_4$ nanopowder was 2 wt.%. The possible reason for the increase in cermet bending strength may be attributed to two facts: the increased relative density and the resultant $Ni_3Si$ distributed in the binder phase during sintering. The as-produced ceramic

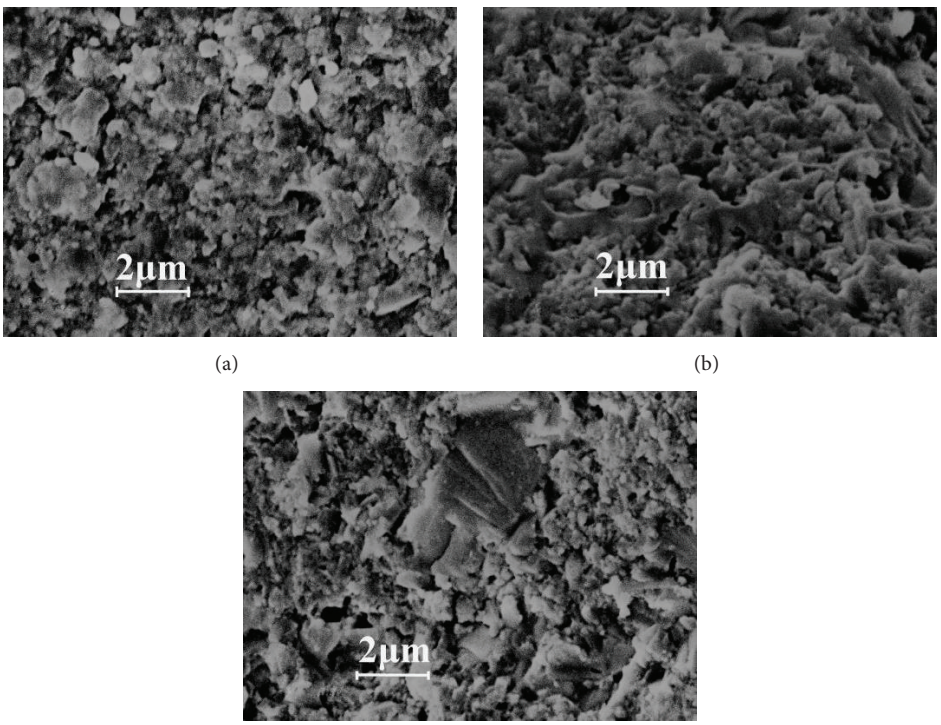


Figure 4: Typical SE SEM images on fracture surface of the as-prepared cermets with different amounts of $Si_3N_4$ nanopowder: (a) 0 wt.%, (b) 2 wt.%, and (c) 5 wt.%.

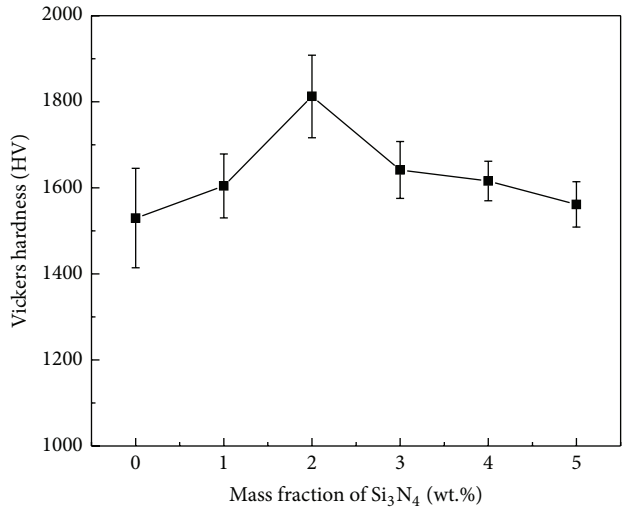


Figure 5: Vickers hardness of the as-prepared TiCN-based cermets as a function of mass fraction of $Si_3N_4$ nanopowder.

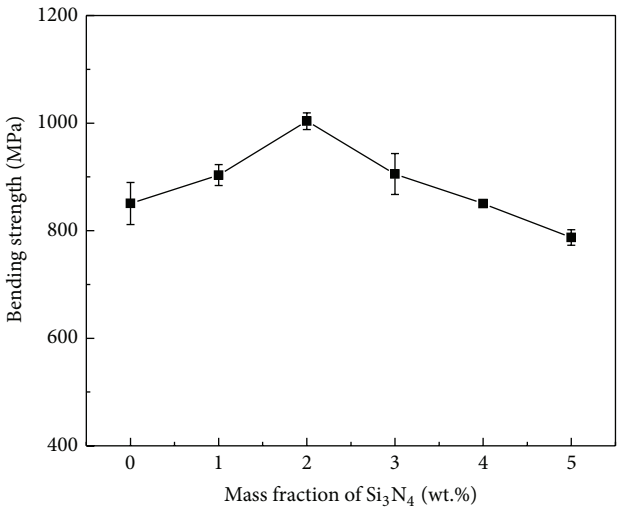


Figure 6: Bending strength of the as-prepared TiCN-based cermets as a function of mass fraction of $Si_3N_4$ nanopowder.

$Ni_3Si$ could inhibit the dislocation motion of metal Ni, and as a result, the binder phase was strengthened and the strength of the TiCN-based cermets was enhanced. Besides, according to [25], the added nanosized particles could locate inside the grains and form a kind of transgranular microstructure, which may deflect the cracks during the fracture. Moreover, there would be some dislocation groups located in those microstructures, which could also hinder the crack extension and lead to their deflection, increasing the fracture energy and thus improving the cermet strength. In this study, the addition of $Si_3N_4$ nanopowder may also produce transgranular microstructure and more subboundaries as shown in Figure 2(b). Since the coefficient of thermal expansion and modulus of elasticity of the added $Si_3N_4$ nanoparticles were

quite misfit with those of the cermets, the residual stress also came into being quite easily in the subboundaries. As the tip of cracks spreads to these areas, this kind of transgranular microstructure could hold up the crack propagation (see in Figure 2(b)); thus, the sample strength was boosted. Nevertheless, as the addition amount of $Si_3N_4$ nanopowder increased, the sample strength decreased as well, which was partially in virtue of the weak bond between the binder phase and hard phase (the spalling as shown in Figure 4(c)). Moreover, the agglomeration of $Si_3N_4$ nanopowder could also weaken the bond between the binder phase and hard phase. Consequently, the whole sample strength dropped down.

## 4. Conclusions

TiCN-based cermets with varied amounts of $Si_3N_4$ nanopowder were fabricated by SPS. No $Si_3N_4$ phase was identified by XRD in the detection limit, but with the addition of $Si_3N_4$ nanopowder, a new phase of $Ni_3Si$ was detected. As the addition amount of $Si_3N_4$ nanopowder increased, the relative density, hardness, and bending strength of the as-prepared samples increased first and then decreased, reaching their maximum of about 98%, 1810 $HV_{10}$, and 1000 MPa, respectively, when the added amount of $Si_3N_4$ nanopowder was 2 wt.%.

## Conflict of Interests

The authors declare that there is no conflict of interests regarding the publication of this paper.

## Acknowledgments

This work was supported by Grand Survey on Land and Nature Sources of China sponsored by China Geological Survey (Grant no. 1212010916026) and National Key Technology R&D Program of China (Grant no. 2011BAB03B08).

## References

[1] Y. Li, N. Liu, X. B. Zhang, and C. L. Rong, "Effect of WC content on the microstructure and mechanical properties of (Ti, W)(C, N)–Co cermets," *International Journal of Refractory Metals and Hard Materials*, vol. 26, no. 1, pp. 33–40, 2008.

[2] S. Cardinal, A. Malchère, V. Garnier, and G. Fantozzi, "Microstructure and mechanical properties of TiC-TiN based cermets for tools application," *International Journal of Refractory Metals and Hard Materials*, vol. 27, no. 3, pp. 521–527, 2009.

[3] P. Ettmayer, H. Kolaska, W. Lengauer, and K. Dreyer, "Ti(C,N) cermets—metallurgy and properties," *International Journal of Refractory Metals and Hard Materials*, vol. 13, no. 6, p. 343, 1995.

[4] Y. Zheng, M. You, W. H. Xiong, W. J. Liu, and S. X. Wang, "Valence-electron structure and properties of main phases in Ti(C, N)-based cermets," *Materials Chemistry and Physics*, vol. 82, no. 3, pp. 877–881, 2003.

[5] S. Q. Zhou, W. Zhao, and W. H. Xiong, "Microstructure and properties of the cermets based on Ti(C, N)," *International Journal of Refractory Metals and Hard Materials*, vol. 27, no. 1, pp. 26–32, 2009.

[6] S. Sugiyama and H. Taimatsu, "Preparation of WC-WB-$W_2B$ composites from $B_4C$-W-WC powders and their mechanical properties," *Materials Transactions*, vol. 43, no. 5, pp. 1197–1201, 2002.

[7] M. Tokita, "Large-size WC/Co functionally graded materials fabricated by spark plasma sintering (SPS) method," *Materials Science Forum*, vol. 423-425, pp. 39–44, 2003.

[8] J. K. Jung and S. H. Kang, "Effect of ultra-fine powders on the microstructure of Ti(CN)-*x*WC-Ni cermets," *Acta Materialia*, vol. 52, no. 6, pp. 1379–1383, 2004.

[9] J. Jung and S. Kang, "Effect of nano-size powders on the microstructure of Ti(C,N)-*x*WC-Ni cermets," *Journal of the American Ceramic Society*, vol. 90, no. 7, pp. 2178–2183, 2007.

[10] N. Liu, J. Zhou, X. B. Zhang, and C. L. Rong, "Effect of powder size on microstructure and mechanical properties of Ti(C,N) based cermets," *Advances in Applied Ceramics*, vol. 106, no. 5, pp. 247–254, 2007.

[11] H. J. Yu, Y. Liu, Y. Z. Jin, and J. W. Ye, "Effect of secondary carbides addition on the microstructure and mechanical properties of (Ti, W, Mo, V)(C, N)-based cermets," *International Journal of Refractory Metals and Hard Materials*, vol. 29, no. 5, pp. 586–590, 2011.

[12] W. Wan, J. Xiong, M. Yang, Z. Guo, G. Dong, and C. Yi, "Effects of $Cr_3C_2$ addition on the corrosion behavior of Ti(C, N)-based cermets," *International Journal of Refractory Metals and Hard Materials*, vol. 31, pp. 179–186, 2012.

[13] W. T. Kwon, J. S. Park, and S. H. Kang, "Effect of group IV elements on the cutting characteristics of Ti(C,N) cermet tools and reliability analysis," *Journal of Materials Processing Technology*, vol. 166, no. 1, pp. 9–14, 2005.

[14] Y. Zheng, W. H. Xiong, W. J. Liu, W. Lei, and Q. A. Yuan, "Effect of nano addition on the microstructures and mechanical properties of Ti(C, N)-based cermets," *Ceramics International*, vol. 31, no. 1, pp. 165–170, 2005.

[15] N. Liu, Y. D. Xu, H. Li, G. H. Li, and L. D. Zhang, "Effect of nano-micro TiN addition on the microstructure and mechanical properties of TiC based cermets," *Journal of the European Ceramic Society*, vol. 22, no. 13, pp. 2409–2414, 2002.

[16] N. Liu, W. Yin, and L. Zhu, "Effect of TiC/TiN powder size on microstructure and properties of Ti(C, N)-based cermets," *Materials Science and Engineering A*, vol. 445-446, pp. 707–716, 2007.

[17] M. Tokita, "Development of large-size ceramic/metal bulk FGM fabricated by spark plasma sintering," *Materials Science Forum*, vol. 308–311, pp. 83–88, 1999.

[18] M. Tokita, M. Kawahara, M. Sonoda, M. Omori, A. Okubo, and T. Hirai, "Preparation and tribological characterization of $ZrO_2$(3Y)+20wt%$Al_2O_3$/SUS410L stainless steel composite functionally graded material fabricated by spark plasma sintering method," *Journal of the Japan Society of Powder and Powder Metallurgy*, vol. 46, no. 3, pp. 269–276, 1999.

[19] S. Sugiyama and H. Taimatsu, "Application of spark plasma sintering to the preparation of advanced materials," *Journal of the Japan Welding Society*, vol. 71, no. 2, pp. 91–94, 2002.

[20] K. Mizuuchi, K. Inoue, M. Sugioka, M. Itami, and M. Kawahara, "Properties of Ti-aluminides-reinforced Ti-matrix laminate fabricated by pulsed-current hot pressing (PCHP)," *Materials Transactions*, vol. 45, no. 2, pp. 249–256, 2004.

[21] S. Grasso, Y. Sakka, and G. Maizza, "Electric current activated/assisted sintering (ECAS): a review of patents 1906–2008," *Science and Technology of Advanced Materials*, vol. 10, no. 5, Article ID 053001, 2009.

[22] K. Mizuuchi, K. Inoue, Y. Agari et al., "Processing of diamond-particle-dispersed silver-matrix composites in solid-liquid co-existent state by SPS and their thermal conductivity," *Composites Part B: Engineering*, vol. 43, no. 3, pp. 1445–1452, 2012.

[23] S. Chao, N. Liu, Y. P. Yuan et al., "Microstructure and mechanical properties of ultrafine Ti(CN)-based cermets fabricated from nano/submicron starting powders," *Ceramics International*, vol. 31, no. 6, pp. 851–862, 2005.

[24] H. Q. Zhang, N. Liu, R. Y. Song, Z. W. Liu, and W. Cai, "Effect of Ni-Co on the properties of ultra-fine grade Ti(C,N)-based cermets," *Cemented Carbide*, vol. 25, no. 4, pp. 214–217, 2008 (Chinese).

[25] Y. Zheng, S. Wang, M. You, H. Tan, and W. Xiong, "Fabrication of nanocomposite Ti(C,N)-based cermet by spark plasma sintering," *Materials Chemistry and Physics*, vol. 92, no. 1, pp. 64–70, 2005.